DOI: 10.1002/anie.200603977

Spin Crossover

A Thermal Spin Transition in a Nanoporous Iron(II) Coordination Framework Material

*Suzanne M. Neville, Boujemaa Moubaraki, Keith S. Murray, and Cameron J. Kepert**

A strong current motivation for the synthesis and characterization of porous coordination framework materials is the incorporation of diverse chemical and physical properties, including multiple properties within the one material.[1,2] Among efforts to achieve advanced functionality in such materials is the introduction of spin-crossover centers to explore possible synergies between spin switching transitions and host–guest chemistry.[1,3–5] Materials of this type provide a new avenue for investigating the spin-crossover phenomenon in the solid state, with guest-exchange being a convenient means for perturbing the framework structure and, therefore, the crossover properties. Such a function promises novel applications in areas such as molecular sensing. Further, these materials offer the possibility of using external stimuli (e.g., temperature, pressure, irradiation) to modify the host–guest chemistry within a uniquely switchable guest environment.[6]

Only a small number of porous spin-crossover systems have been reported to date, each of these containing iron(II) centers bridged by either dipyridyl[3,4] or cyanometallate[5] ligands. Previously, we reported the nanoporous phase $[Fe(NCS)_2(azpy)_2]\cdot{}^1/_2\{guest\}$ (azpy = 4,4′-azopyridine), which undergoes a spin-crossover transition that is sensitive to the presence of included guest molecules.[3] Herein, we incorporate the bridging ligand 2,3-bis(4′-pyridyl)-2,3-butanediol (bpbd; Figure 1) into a new spin-crossover coordination framework material, $[Fe(NCS)_2(bpbd)_2]\cdot\{acetone\}$ (**A·{ac}**), with the aim of targeting potential host–host and host–guest hydrogen-bonding interactions provided by the diol functional groups of the ligand. This hydrogen-bonding potential is desirable, firstly, to enhance host framework stability.[7] Secondly, hydrogen-bonding interactions have been shown to influence both the temperature and nature of spin transitions through their influence on the coordination environment and on the cooperativity between coordination sites.[3,8]

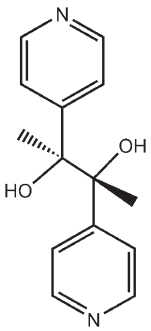

Figure 1. The ligand 2,3-bis(4′-pyridyl)-2,3-diol (bpbd).

Single crystals of **A·{ac}** were grown by slow diffusion in acetone and their structure determined by X-ray diffraction. The iron(II) coordination sphere consists of axial thiocyanate ligands bound through the terminal nitrogen atom and four equatorial pyridyl (py) donor groups from four separate bpbd ligands. These bpbd ligands bridge the iron centers to form extended two-dimensional (4,4) rhombic grids of diagonal dimensions 17.9×20.6 Å^2. Structurally equivalent two-dimensional grids interpenetrate at an angle of 90° (Figure 2), resulting in a pseudo three-dimensional structure with square one-dimensional channels along the *c* axis of dimensions 14.5×14.5 Å^2 (Figure 3). The channels account for 27.3 % of

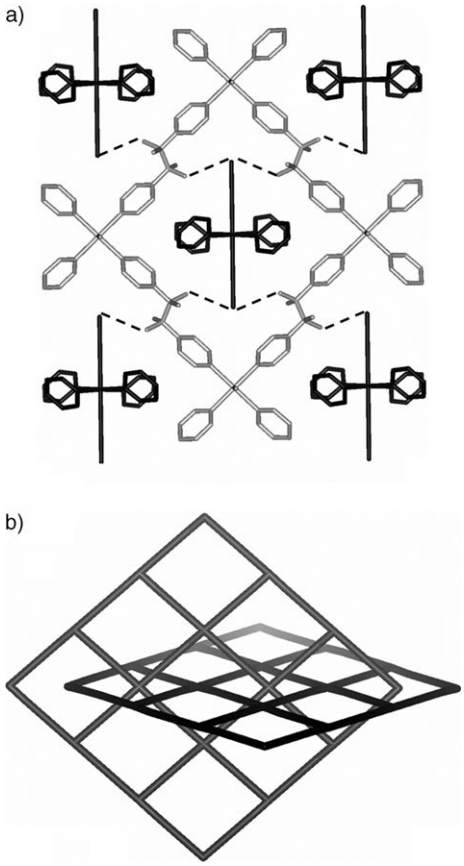

Figure 2. a) The interpenetrated rhombic grid structure of **A·{ac}**; hydrogen-bonding interactions (dashes) between the diol groups on the bpbd ligand on one grid (gray) and the thiocyanate groups on a series of perpendicular, interpenetrating grids (black) are shown. b) A topological representation of the orthogonal interpenetration of the rhombic grids.

[*] Dr. S. M. Neville, Prof. C. J. Kepert
School of Chemistry
University of Sydney
Sydney, 2006 (Australia)
Fax: (+61) 2-9351-3329
E-mail: c.kepert@chem.usyd.edu.au
Dr. B. Moubaraki, Prof. K. S. Murray
School of Chemistry
Monash University
Victoria, 3800 (Australia)

Supporting information for this article is available on the WWW under http://www.angewandte.org or from the author.

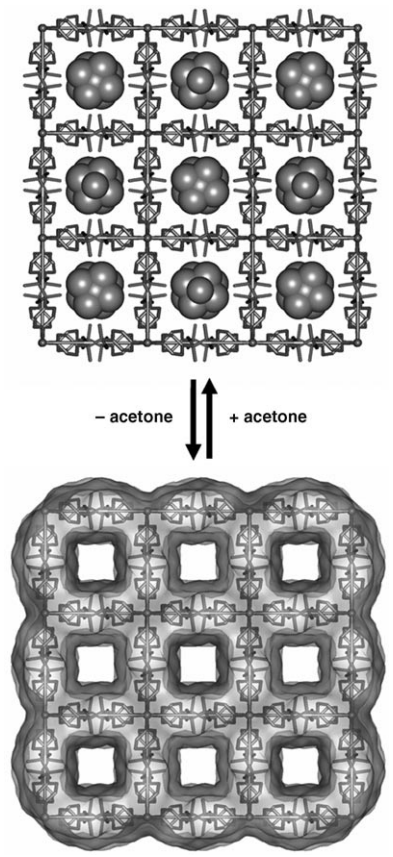

Figure 3. Desorption of acetone guest molecules (space-filling representation) from **A·{ac}** (top) to form **A** (bottom) proceeds by a single-crystal-to-single-crystal structural transformation in which the framework host structure is essentially unaltered. The apohost **A**, which is shown with a van der Waals surface to indicate the one-dimensional pore structure, houses empty channels that occupy just over 27% of the crystal volume.

the total crystal volume and are filled with solvent acetone in the as-grown material.

The interpenetrated framework structure[9,10] is stabilized by hydrogen bonding interactions between the diol groups of the bpbd ligands and the sulfur atoms of thiocyanate groups from the interpenetrated grid (O(H)···S: 3.317(3) Å; Figure 2a). Such a feature is not present in the isotopological spin-crossover frameworks with azpy[3] and *trans*-1,2-bis(4′-pyridyl)ethylene (tvp)[4] bridges. The guest acetone molecules, which are disordered but could be located and refined structurally, do not participate in any short hydrogen-bonding interactions with the diol groups from the bpbd ligands, even though these groups protrude into the pores. This situation contrasts to that observed in a framework containing a similar ligand, 1,2-bis(4′-pyridyl)-1,2-ethanediol, in which hydrogen-bonding interactions to guest water are reported.[11]

Thermogravimetric analysis of **A·{ac}** revealed the complete, reversible removal of guest acetone between 20 and 40 °C to form the apohost, **A** (see the Supporting Information, Figures S3 and S4). The structural consequences of desorption were probed by single-crystal X-ray diffraction, with heating to 102 °C to achieve complete guest desorption. Structural analysis of **A**[12] revealed minimal deviation of the framework atoms between the solvated and desolvated states. The most significant variation is a decrease in the dihedral angle of the pyridyl groups through the iron(II) center from 66.3 to 64.1°. The pronounced structural stability to desolvation can be attributed to the extensive interframework hydrogen-bonding network described above, which is present and of similar geometry in both the solvated and desolvated states (O(H)···S: 3.317(3) and 3.308(10) Å for **A·{ac}** and **A**, respectively).

Magnetic susceptibility measurements of **A·{ac}** revealed a relatively abrupt one-step full spin transition, with $T_{1/2} = 162$ K (Figure 4a). The $\chi_M T$ values remained approximately

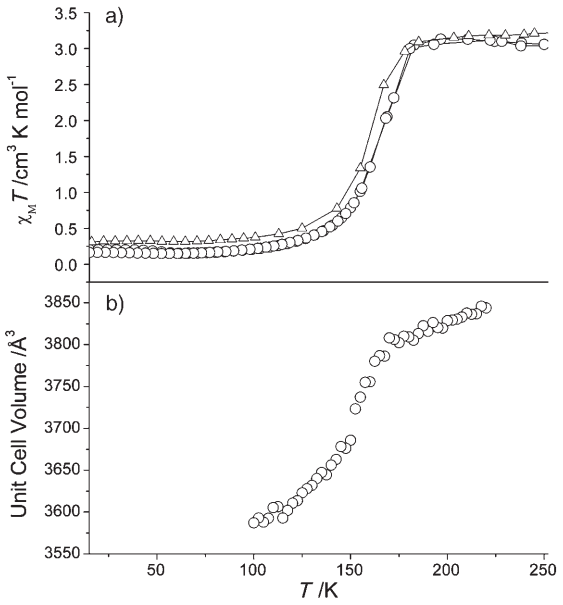

Figure 4. a) The temperature-dependent magnetic susceptibility for **A·{ac}** (○) and **A** (▽). b) The unit-cell volume evolution over the spin transition versus temperature for a single crystal of **A·{ac}** (○).

constant at 3.2 cm^3 K mol^{-1} between 200 and 300 K, which is within the range of values expected for high-spin (hs) iron(II). Below 200 K, the magnetic moment decreased rapidly, and then more gradually, reaching a constant value of 0.14 cm^3 K mol^{-1} below 100 K. This result is consistent with a complete spin conversion; a small amount of residual paramagnetism is common in spin-crossover systems and can be attributed to surface and site defects and to temperature-independent paramagnetic susceptibility in the iron(II) low-spin (ls) centers. The transition is considerably more abrupt than those of the isotopological azpy-[3] and tvp-bridged[4] frameworks, a feature we attribute to an enhanced cooperativity between the iron(II) centers conferred by the network of interframework hydrogen-bonding interactions. No hysteresis was observed in the $\chi_M T$ values when the temperature was raised slowly in the 100 to 200 K region. Upon quench cooling a small amount of spin-state trapping was observed below 50 K.

The unit-cell parameters of **A·{ac}** were monitored over the course of the spin transition using single-crystal X-ray

diffraction and show features similar to that observed in the temperature-dependent magnetic susceptibility studies (Figure 4b and Supporting Information, Figure S2). A steady decrease in each of the unit-cell parameters is observed between 220 and 170 K, with an overall decrease in the unit-cell volume of approximately 4%. Full structural characterizations were carried out above the spin transition, $\mathbf{A}^{hs}$**·{ac}** (220 K),[9] and below the spin transition, $\mathbf{A}^{ls}$**·{ac}** (100 K),[10] allowing the structural consequences of the spin crossover to be determined. The overall structural motif of the material remains unchanged over the transition. From the high-spin to low-spin states, a contraction in average Fe–N bond length of 0.18 Å is observed, consistent with a full spin transition (Fe–N(CS) 2.108(6) (220), 1.941(9) Å (100 K) and Fe–N(py) 2.213(3) (220), 2.032(6) Å (100 K)). There is a concomitant decrease in the pore dimensions from 14.5×14.5 to 14.2×14.2 Å^2 and, consequently, a 5% decrease in the solvent-accessible void volume (equating to a drop from 27.3 to 25.1% of the crystal volume).

Magnetic-susceptibility measurement of the apohost framework, **A**, demonstrated spin-crossover behavior that is remarkably similar to that of the guest-containing phase, **A·{ac}** (Figure 4a). There is a slight decrease in temperature of the transition from $T_{1/2}=162$ K in **A·{ac}** to 156 K in **A**, whilst other aspects of the transition remain essentially unchanged. The retention of similar spin-crossover properties with guest removal contrasts markedly with the behavior of other materials of this general type.[3,5] These materials most notably include $[Fe(NCS)_2(azpy)_2]\cdot{}^1/_2\{EtOH\}$, which undergoes a one-step "half" spin transition that is lost upon ethanol desorption;[5] in situ structural analysis of this phase revealed considerable changes to the iron(II) coordination environment associated with the loss of host–guest hydrogen-bonding interactions and with the rotation of azpy ligands as the framework collapsed partially. The retention of similar spin-crossover behavior with conversion of **A·{ac}** to **A** can be attributed jointly to the absence of short host–guest interactions in **A·{ac}** and to the presence of interframework hydrogen-bonding interactions, the latter imparting considerable robustness of the host lattice and being maintained in the presence and absence of the guests. The slight decrease in transition temperature with guest removal suggests a small perturbation of the ligand-field splitting at the iron(II) center arising from the subtle steric and electronic influence of the guest; the electronic influence contains a dielectric component.

In conclusion, we observe a retention of spin-crossover behavior in a robust nanoporous coordination framework after guest desorption and attribute this to the comparatively minor influence of the guest molecule on the coordination environment of the iron(II) crossover centers. Interframework hydrogen-bonding interactions in **A·{ac}** provided by the diol functional groups on the ligand appear to play an integral role in providing structural stability and inflexibility to the host lattice and in favoring a relatively abrupt spin-crossover transition. The generation of highly robust and porous molecular materials provides an as yet unexplored method for investigating the influence of coordination environment and host–guest interactions on spin-transition behavior. We are currently carrying out extensive investigations of this and other related materials in which variations in the dipyridyl bridging ligand, the anion $[NCX]^-$ (X = S, Se, BH_3), and the guest solvent molecule are made.

Experimental Section

Crystals of **A·{ac}** were grown by slow diffusion of a solution of bpbd (38.3 mg, 0.157 mmol; obtained from Aldrich as a 97% *meso* and 3% *rac* isomeric mixture, as determined by HPLC) in acetone with a solution of $Fe(ClO_4)_2\cdot H_2O$ (20 mg, 0.078 mmol) and NH_4NCS (11.9 mg, 0.156 mmol) in acetone in an H-shaped vessel. Orange crystals of **A·{ac}** formed in 60% yield over two weeks.

Data for all the structures were measured on a Bruker SMART CCD diffractometer ($Mo_{K\alpha}$ radiation $\lambda=0.71073$ Å) equipped with an Oxford Systems Cryostream. Empirical absorption corrections were applied using the SADABS program.[13] Non-hydrogen atoms were refined anisotropically and hydrogen atoms were affixed using the riding model. CCDC-610087 ($\mathbf{A}^{hs}$**·{ac}**), CCDC-610088 ($\mathbf{A}^{ls}$**·{ac}**), and CCDC-610089 (**A**) contain the supplementary crystallographic data for this paper. These data can be obtained free of charge from The Cambridge Crystallographic Data Centre via www.ccdc.cam.ac.uk/data_request/cif.

Received: September 28, 2006
Published online: February 15, 2007

Keywords: host–guest systems · iron · metal–organic framework · microporous materials · spin crossover

[1] a) C. J. Kepert, *Chem. Commun.* **2006**, 695–700; b) S. Kitagawa, R. Kitaura, S. Noro, *Angew. Chem.* **2004**, *116*, 2388–2430; *Angew. Chem. Int. Ed.* **2004**, *43*, 2334–2375.

[2] a) N. R. Champness, *Dalton Trans.* **2006**, 877–880; b) S. L. James, *Chem. Soc. Rev.* **2003**, *32*, 276–288; c) C. Janiak, *Dalton Trans.* **2003**, 2781–2804; d) M. J. Rosseinsky, *Microporous Mesoporous Mater.* **2004**, *73*, 15–30; e) C.-T. Chen, K. S. Suslick, *Coord. Chem. Rev.* **1993**, *128*, 293–322; f) M. Kurmoo, H. Kumagai, K. W. Chapman, C. J. Kepert, *Chem. Commun.* **2005**, 3012–3014.

[3] G. J. Halder, C. J. Kepert, B. Moubaraki, K. S. Murray, J. D. Cashion, *Science* **2002**, *298*, 1762–1765.

[4] J. A. Real, E. Andres, M. C. Muñoz, M. Julve, T. Granier, A. Bousseksou, F. Varret, *Science* **1995**, *268*, 265–267.

[5] a) V. Niel, A. L. Thompson, M. C. Muñoz, A. Galet, A. S. E. Goeta, J. A. Real, *Angew. Chem.* **2003**, *115*, 3890–3893; *Angew. Chem. Int. Ed.* **2003**, *42*, 3760–3763; b) S. Bonhommeau, G. Molnár, A. Galet, A. Zwick, J. A. Real, J. J. McGarvey, A. Bousseksou, *Angew. Chem.* **2005**, *117*, 4137–4141; *Angew. Chem. Int. Ed.* **2005**, *44*, 4069–4073.

[6] K. S. Murray, C. J. Kepert, *Top. Curr. Chem.* **2004**, *233*, 195–228.

[7] a) C. J. Kepert, M. J. Rosseinsky, *Chem. Commun.* **1999**, 375–376; b) G. J. Halder, C. J. Kepert, *J. Am. Chem. Soc.* **2005**, *127*, 7891–7900; c) N. L. Rosi, M. Eddaoudi, J. Kim, M. O'Keeffe, O. M. Yaghi, *CrystEngComm* **2002**, *4*, 401–404; d) P. V. Ganesan, C. J. Kepert, *Chem. Commun.* **2004**, 2168–2169; e) K. Uemura, S. Kitagawa, K. Fukui, K. Saito, *J. Am. Chem. Soc.* **2004**, *126*, 3817–3828; f) S. R. Batten, R. Robson, *Angew. Chem.* **1998**, *110*, 1558–1595; *Angew. Chem. Int. Ed.* **1998**, *37*, 1460–1494; g) S. Kitagawa, K. Uemura, *Chem. Soc. Rev.* **2005**, *34*, 109–119; h) G. J. Halder, C. J. Kepert, *Aust. J. Chem.* **2006**, *59*, 597–604.

[8] a) J. A. Real, A. B. Gaspar, V. Niel, M. C. Muñoz, *Coord. Chem. Rev.* **2003**, *236*, 121–141; b) P. Gütlich, Y. Garcia, H. Goodwin,

Chem. Soc. Rev. **2000**, *29*, 419 – 427; c) P. Gütlich, H. A. Goodwin, *Top. Curr. Chem.* **2004**, *233*, 1 – 47.

[9] Crystal data for $\mathbf{A}^{hs}$**·{ac}**: $Fe_2C_{63}H_{70}N_{12}O_9S_4$, $M_r = 1379.25$, orange rod, crystal dimensions $0.28 \times 0.12 \times 0.12$ mm^3, tetragonal, *P*4/*ncc* (no. 130), $a = 14.574(3)$, $b = 14.574$, $c = 17.964(4)$ Å, $V = 3815.6(11)$ Å^3, $T = 220$ K, $Z = 2$, $\rho_{calcd} = 1.200$ g cm^{-3}, $\mu(Mo_{K\alpha}) = 0.545$ mm^{-1}, $GoF = 1.037$, 1156 observed ($I > 2\sigma(I)$), $R1(F) = 0.0711$, $wR2(F^2) = 0.1853$.

[10] Crystal data for $\mathbf{A}^{ls}$**·{ac}**: $Fe_2C_{63}H_{70}N_{12}O_9S_4$, $M_r = 1379.25$, purple rod, crystal dimensions $0.28 \times 0.12 \times 0.12$ mm^3, tetragonal, *P*4/*ncc* (no. 130), $a = 14.2240(17)$, $c = 17.580(4)$ Å, $V = 3556.8(10)$ Å^3, $T = 100$ K, $Z = 2$, $\rho_{calcd} = 1.288$ g cm^{-3}, $\mu(Mo_{K\alpha}) = 0.585$ mm^{-1}, $GoF = 1.366$, 990 observed ($I > 2\sigma(I)$), $R1(F) = 0.0831$, $wR2(F^2) = 0.1919$.

[11] a) M. Kondo, T. Okubo, A. Asami, S. Noro, T. Yoshitomi, S. Kitagawa, T. Ishii, H. Matsuzaka, K. Seki, *Angew. Chem.* **1999**, *111*, 190 – 193; *Angew. Chem. Int. Ed.* **1999**, *38*, 140 – 143; b) M. Kondo, A. Asami, H. Chang, S. Kitagawa, *CrystEngComm* **1999**, *2*, 115 – 122.

[12] Crystal data for **A**: $Fe_2C_{60}H_{64}N_{12}O_8S_4$, $M_r = 1321.17$, orange rod, crystal dimensions $0.44 \times 0.18 \times 0.18$ mm^3, tetragonal, *P*4/*ncc* (no. 130), $a = 14.7260(10)$, $c = 17.899(3)$ Å, $V = 3881.5(7)$ Å^3, $T = 375$ K, $Z = 2$, $\rho_{calcd} = 1.130$ g cm^{-3}, $\mu(Mo_{K\alpha}) = 0.532$ mm^{-1}, $GoF = 1.117$, 916 observed ($I > 2\sigma(I)$), $R1(F) = 0.0700$, $wR2(F^2) = 0.2678$.

[13] SMART, SAINT, and XPREP, Area-detector control and data integration and reduction software, Bruker AXS Inc., Madison, Wisconsin (USA), **1995**; G. M. Sheldrick, SADABS, Program for scaling and correction of area detector data, University of Göttingen (Germany), **1996**.

